Original paper

Fast discrimination and counting of filled/unfilled rice spikelets based on bi-modal imaging

Lingfeng Duan, Wanneng Yang, Kun Bi, Shangbin Chen, Qingming Luo, Qian Liu *

Britton Chance Center for Biomedical Photonics, Wuhan National Laboratory for Optoelectronics-Huazhong University of Science and Technology, Wuhan 430074, China

ARTICLE INFO

ABSTRACT

Spikelets per panicle and grains per panicle (also known as filled spikelets per panicle), directly contributing to rice yield, are two imperative traits that need to be evaluated in yield-related research. Current determination of total spikelet number and filled spikelet number are generally measured manually, which is tedious and subjective. This paper proposes a new method of counting total spikelets and filled spikelets simultaneously, based on automatic discrimination of filled and unfilled spikelets by combining visible light imaging and soft X-ray imaging. Visible light imaging was applied to measure the projected area of the spikelet hull, while soft X-ray imaging yielded the projected area of the inner brown rice kernel. The filling rate, defined as the area ratio of rice kernel to hull, was used to discriminate the filled and unfilled spikelets. 29 panicle samples were tested to evaluate the efficiency and accuracy. The results showed that the counting efficiency was approximately 2000 spikelets/min. The root mean squared error (RMSE) was 0.42 for total spikelet number and 0.77 for filled spikelet number. The mean absolute percentage errors (MAPE) were 0.22% and 0.80% for each, respectively. The method shows great potential in improving the efficiency of trait evaluation in plant breeding and genetic research, as well as serving for crop phenomics.

1. Introduction

High yield has been a major breeding target in cereals, including rice (Zhang, 2007; Wang et al., 2008) which is the staple food for approximately half of the world's population (Lian et al., 2005). Yield of a rice plant is determined by the product of grain weight, number of grains per panicle and number of panicles per plant (Xing and Zhang, 2010). Number of grains per panicle, also called filled spikelets per panicle (Yoshida, 1981), and spikelets per panicle are two key traits in rice research, for example yield-related quantitative-trait-loci analysis (Xiao et al., 1998; Thomson et al., 2003; Tian et al., 2006) and stress-tolerance research (Bohra and Doerffling, 1993; Prasertsak and Fukai, 1997; Yang et al., 2001).

To obtain the number of spikelets and filled spikelets, researchers usually depend on manual counting, which is time-consuming and labor-intensive. The water-selection method, in which the sinking spikelets are regarded as filled spikelets, is a popular manual method to separate filled spikelets from unfilled spikelets (Ying et al., 1998; Yang et al., 2000). Alternatively, the wind-selection method uses a seed blower to discriminate filled

and unfilled spikelets (Tirol-Padre et al., 1996; Bueno and Lafarge, 2009). After the separation, either by water-selection method or wind-selection method, the filled and unfilled spikelets can be counted. However, both manual methods give subjective and inconsistent results. Therefore, it is essential to develop an automated method that can discriminate and count spikelets with more objective, accurate and consistent measurements.

At present, the automatic seed counting machine, which can count seeds including spikelets by accumulating photoelectric pulses generated by a photoelectric switch, are commercially available. However, instead of discriminating filled and unfilled spikelets and counting them separately, a typical commercial seed counter only measures the total number of spikelets. Moreover, the efficiency of the machine is substantially limited because the spikelets have to pass through the detection device one by one. For instance, the 801 Model Count-A-Pak Seed Counter (SEEDBURO Equipment Company, USA) has a counting speed of approximately 550 seeds per minute (http://www.seedburo.com/prod_lit/categ07/CountAPak07lit.pdf). In addition, the photoelectric switch fails to discriminate impurities from spikelets. To obtain both filled spikelet number and total spikelet number, the user has to manually separate filled and unfilled spikelets before counting. Therefore, there is an urgent need for a method that can simultaneously count filled spikelet number and total spikelet number without need for

the time-consuming manual separation of filled and unfilled spikelets.

Machine vision has advantages in accuracy, consistency and objectivity, and thus has been widely used in the grain industry (Crowe et al., 1997; Wan et al., 2002; Neethirajan et al., 2007a; Venora et al., 2009). Visible light imaging is one of the popular imaging techniques in machine vision to obtain the external appearance of grains. Prior studies by Zayas et al. (1989) used visible light images to discriminate wheat from non-wheat components. Luo et al. (1999) developed a color machine vision system to identify healthy and six types of damaged kernels. Manickavasagan et al. (2008) established a machine vision system with a monochrome camera to identify eight western Canadian wheat classes. However, visible light imaging cannot penetrate opaque objects and thus is not capable of revealing internal structures. Unlike visible light, soft X-rays with electromagnetic wavelengths ranging from 1 to 100 nm (Neethirajan et al., 2007b) have a relatively greater penetration, and thus reveal the internal density distribution of seeds with high contrast. Soft X-ray imaging has been widely applied to detect internal damage and infestation in wheat kernels (Haff and Slaughter, 2004; Karunakaran et al., 2004; Fornal et al., 2007). These studies have utilized high performance X-ray systems and acquired images under static situation (both X-ray system and grains are motionless) to generate good quality grain images with high contrast and signal to noise ratio (SNR). During real-time imaging of moving grains (line-scan imaging), however, it is difficult to get high quality X-ray image due to low X-ray attenuation by spikelets.

The degree of filling of a spikelet is variable. In this study, the projected area ratio of brown rice kernel, hereafter termed rice kernel, to spikelet hull, termed filling rate (*FR*), is utilized as an indicator of the degree of filling. Visible light imaging can measure the projected area of spikelet hull, whereas cannot obtain the projected area of rice kernel due to the fact that visible light cannot penetrate the opaque spikelet hull. Ideally, the X-ray imaging can simultaneously obtain both the projected area ratio of a rice kernel and the hull area if the contrast and SNR of the X-ray image were sufficiently high. However, spikelet has a very low attenuation for X-ray, even lower than several commercial conveyor materials such as cotton canvas, nylon and PVC. Consequently, it is hard to generate a high quality X-ray image in line-scan imaging. In addition, a typical high-performance X-ray system costs about three times more than a low-performance system. Moreover, high resolution is needed for distinguishing the thin spikelet hull, which will either decrease the field of view or require an even more expensive X-ray system with a detector of larger size. To overcome above difficulties, bi-modal imaging is deployed in this study to discriminate filled spikelets and unfilled spikelets, with visible light imaging acquiring the projected area of the spikelet hull, while soft X-ray imaging obtains the area of the rice kernel.

This paper, to the best of our knowledge, is the first to introduce and test an automated machine for simultaneously counting filled spikelet number and total spikelet number, with no need for the time-consuming manual separation of filled spikelets and unfilled spikelets. The focus of this paper is on the discrimination method for unfilled spikelets and filled spikelets.

The objective of this work was to explore and demonstrate the concept of combining visible light imaging and soft X-ray imaging in automatic discrimination and counting of unfilled and filled spikelets. The task involved the design of a prototype system for imaging rice on a conveyor belt, the development of a real-time algorithm for co-registering X-ray detector and CCD camera, the development of real-time machine vision algorithms for discrimination of filled spikelets and unfilled spikelets, and the design of a communication interface for displaying the resultant images and data.

Table 1
Main characteristics of the line-scan X-ray detector.

Main characteristics	X-scan 0.4f3-205
X-ray tube voltage range (kV)	20–160
Scintillator material	GOS/CWO
Number of pixels	768
Pixel pitch (mm)	0.4
Pixel height (mm)	0.6
Pixel width (mm)	0.3
Maximum scanning speed (mm/s)	800
A/D resolution (bit)	14
Saturation signal/RMS noise	>2000

2. Materials and methods

2.1. Sample preparation and manual measurement

29 rice panicle samples were tested to evaluate the accuracy of the method. Rice panicles were first subjected to a threshing machine, after which raw materials, mainly comprised of unfilled spikelets, filled spikelets and small pieces of branches, were collected for testing.

Filled spikelets and unfilled spikelets were separated using the water-selection method, after which the samples were sun-dried and counted separately by skilled workers. The total spikelet number and the filled spikelet number for each panicle were recorded as reference data.

2.2. Experimental set-up

The implemented prototype consists of a feeding unit, an inspection unit and a gathering unit, which are described in the following subsections.

2.2.1. Feeding unit

Spikelets were fed into the inspection machine through a stainless-steel hopper. A vibratory feeder was used to arrange the spikelets as a single layer and separate individual spikelet. This step was instrumental for the subsequent processes, since it facilitated image analysis. Subsequently, the spikelets were transferred onto a 250 mm wide where the ellipsoidal spikelets lay flat.

2.2.2. Inspection unit

A line-scan charge coupled device(LCCD) camera (Tapix LCD 2048@9000, TATTILE International Ltd., Italy), equipped with a 28 mm lens (F1.8 EX DG Aspherical Macro, SIGMA, Japan), was used to acquire a visible-light image with 2000 × 2048 pixel and the resolution of 0.19 mm/pixel. The camera was controlled by the computer workstation (HP xw6400, Hewlett-Packard Development Company, USA) through a frame grabber card (NI PCI-1426, National Instruments Corporation, USA) that digitized the images into 3-color 8-bit files. A line-array LED (BL-494-40-W, Cogstek Automation Technology Co. Ltd., China; set to 28 V voltage and 1.5 A current) served as the light source of the visible light imaging system.

The X-ray imaging system was comprised of a fan-beam X-ray source (T80-1-60, BMEI Co. Ltd., China) and a line-scan X-ray detector (X-Scan 0.4-205, BMEI Co. Ltd., China). The X-ray source possessed a focal spot size of about 0.8 mm with an affixed tungsten anode. Tube voltage range and tube current range of the X-ray source were 40–80 kV and 0.2–1 mA, respectively. Details pertaining to the linear-array detector used in the system are shown in Table 1. The X-ray detector was directly connected to the computer via a USB 2.0 port, which acquired a 16-bit 1000 × 768 pixel grayscale X-ray image (termed X-ray image), with resolution of 0.36 mm/pixel.
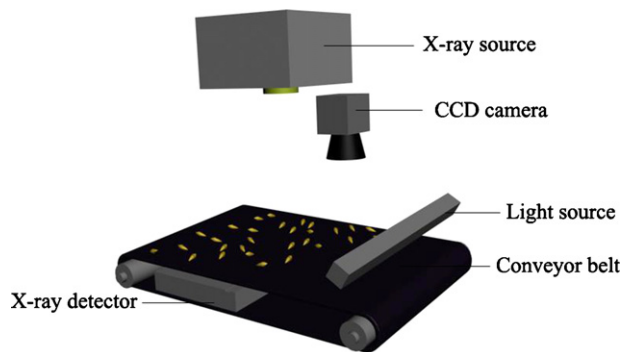
Fig. 1. Experimental set-up diagram. Both the CCD camera and X-ray detector are line-scan devices. The line-scan CCD camera, line-array LED light source and X-ray source are placed over the conveyor belt, while the X-ray detector below it.

In order to minimize the X-ray attenuation of the conveyor belt, cloth was chosen as the belt material. Moreover, compared with other colors, black cloth can provide a visible light image with higher contrast, which aided the image processing. The scheme of the main elements of the machine is shown in Fig. 1. The LCCD camera, the line-array LED, and the X-ray source were placed over the conveyor belt, while the X-ray detector is underneath.

A primary limiting factor to improve the spikelet counting efficiency was the speed of the X-ray imaging. Higher imaging speed was a plus in terms of throughput, but the consequence was worse X-ray image quality, which directly affected the identification accuracy for filled spikelets. After taking into account both the counting speed and the identification accuracy, a 10 ms integration time was chosen for the X-ray detector in the experiments. The conveyor speed and CCD line rate were adjusted in accordance with X-ray imaging speed, allowing both X-ray detector and CCD camera to grab undeformed images.

2.2.3. Gathering unit

After inspection, spikelets were transferred from the conveyor by falling into a gathering unit where they were collected and packed.

2.3. Image acquisition

In the beginning of the measurement, the worker pressed a button to send a signal to the computer through the serial port, which automatically started the conveyor. Meanwhile, the LCCD camera and X-ray detector were triggered simultaneously for continuous image acquisition. Subsequently, spikelets were inputted through the feeding unit and imaged as they passed through the inspection unit. Images were acquired and stored using NI-IMAQ VI Library for LabVIEW (National Instruments Corporation, USA). The red (R) component was extracted from the color image to form an 8-bit monochromatic grayscale image, as color information was not necessary due to the high contrast.

This paper focused on determining the potential of combining bi-modal imaging for discrimination of filled spikelets and unfilled spikelets. Experiments were carried out to examine accuracy of the method rather than the implemented prototype machine. In order to eliminate counting errors caused by the conveying equipment, the spikelets were randomly placed on the conveyor belt manually, one panicle at a time. In practical measurements, spikelets were fed into the machine through the feeding unit.

2.4. Image analysis

The image analysis algorithm flow chat is shown in Fig. 2. The main procedure included image segmentation, watershed segmen-
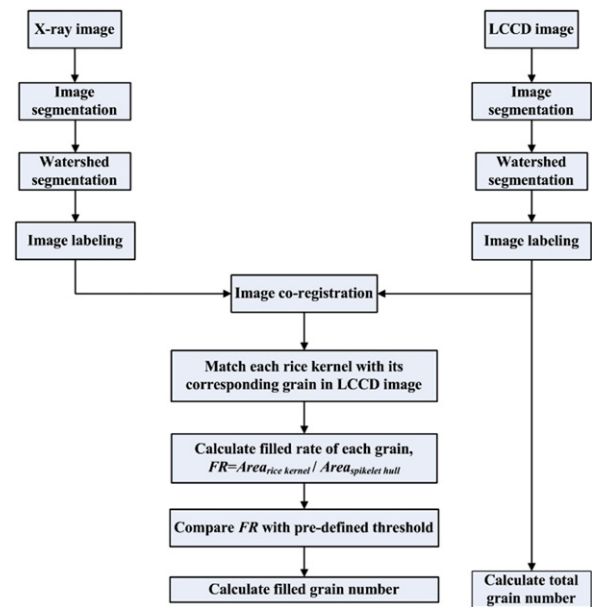

Fig. 2. Image analysis algorithm flow chart.

tation for touching objects, image labeling, image co-registration, and unfilled and filled spikelets discrimination and counting.

All the image analysis algorithms were programmed using NI Vision for LabVIEW 8.6 (National Instruments Corporation, USA), with the exception of distance transformation, grayscale reconstruction and watershed segmentation algorithm, which were programmed using C language and compiled into a dynamic-link library (dll) for LabVIEW calling.
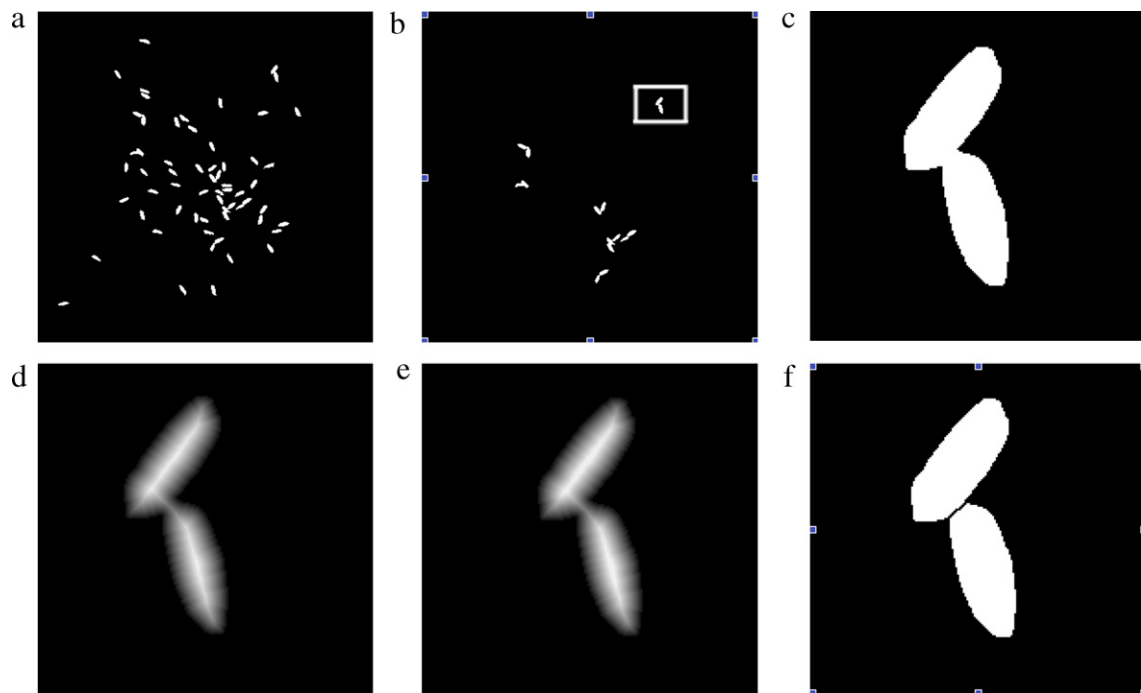
2.4.1. Image segmentation

The image segmentation was carried out after the image calibration. The aim of image segmentation was to obtain a binary image (the object points were assigned 1 and the background points assigned 0) and remove unwanted objects.

The LCCD image was segmented into a binary image using a fixed threshold. Median filter with a 3×3 neighborhood was used to remove isolated pixels. To further minimize noises, small objects were removed from segmented images. As area of noises was usually much smaller than spikelets, objects having area less than one half of the spikelets were regarded as noises. After small objects were removed, the length–width ratio was calculated for all objects. Objects with a length–width ratio larger than five times the average ratio were reckoned to be unwanted objects which are mostly small piece of branch.

Image enhancement, more specifically, a linear transformation was performed to sharpen the contrast of X-ray image by evenly distributing a given gray-level interval [rangeMin, rangeMax] over the full gray scale $[-32,768, 32,767]$ (16-bit signed integer). An automatic local thresholding algorithm, named background correction algorithm was used for X-ray image segmentation. The background correction algorithm categorizes a pixel based on the gray value statistics of its neighboring pixels. A 32×32 window size was used in the algorithm. Similar to the LCCD image analysis, isolated pixels in the X-ray image were removed by a median filter with a 3×3 neighborhood. By comparing the area of objects with an area threshold, noises were further removed.

More details concerning background correction algorithm may be found in NI Vision concepts manual (National Instruments Corporation, USA).

Fig. 3. Watershed segmentation procedure: (a) original binary image of the spikelets; (b) touching kernels extracted from (a); (c) magnified image for kernels in the rectangle in (b); (d) binary image in (c) after distance transform; (e) grayscale reconstruction of (d); (f) watershed segmentation result.

2.4.2. Watershed segmentation

In real-time applications, the spikelets were likely to be touching, which needed to be further segmented. Watershed segmentation (Vincent and Soille, 1991), based on a distance transformation, was applied in this study to segment touching objects in the image. The detailed procedure was described as follows:

Step 1: Touching objects were discriminated from isolated objects.
Step 2: Distance transformation dist(I), in which gray value of each pixel in the resultant image is the shortest distance between the pixel and background (Paglieroni, 1992), was performed on the image I that contains only touching objects.
Step 3: To minimize the over-segmentation phenomenon of watershed segmentation algorithm, the distance function dist(I) was reconstructed from dist(I) − 1 by using a grayscale reconstruction algorithm (Vincent, 1992, 1993).
Step 4: The inverse of the reconstructed image was calculated.
Step 5: Watershed segmentation algorithm was carried out on the reconstructed image.

Fig. 3 illustrates the watershed segmentation procedure. A discrimination procedure was performed on the binary image (Fig. 3a) to extract the touching kernels (Fig. 3b). Fig. 3c shows the magnified image for kernels in the boxed region of Fig. 3b. The two-dimensional Euclidean distance transform of the binary touching kernel image was calculated afterwards (Fig. 3d). Subsequently, grayscale reconstruction was conducted (Fig. 3e). In the end, watershed segmentation was applied (Fig. 3f).

2.4.3. Image labeling

To mark each object for matching, the two binary images were labeled. Each object was labeled according to its position, from top to bottom and left to right. For instance, the top left object was labeled as 1. Fig. 4 shows the original image, segmented binary image and labeled image for both LCCD and X-ray image. The labeled image was shown using the pseudo color method for better visualization. In addition, the total number of spikelets that equals to the maximum labeling number in the LCCD image was calculated after image labeling.

2.4.4. Image co-registration

Prior to the experiment, the LCCD and X-ray cameras were co-registered using a steel plate with a grid of 10 mm spaced dots. After imaging the plate with both the CCD camera and X-ray system, a registration algorithm learned the relative coordinates of the fields of view of the two imaging systems. This learning phase of the co-registration was accomplished using NI Vision Assistant 8.6 (National Instruments, USA). Subsequently during the experiments, the registration algorithm interpreted the two images such that the location of a spikelet hull in the LCCD image corresponded to the rice kernel of the same spikelet in the X-ray image.

Simple co-registration required that two assumptions were met: (1) the conveyor ran at an absolutely constant speed, and (2) the CCD camera and X-ray detector started acquiring images with exactly the same time delay after an acquisition instruction was sent. However, in practical measurements, the conveyor speed fluctuated within a narrow range, and the response time of the CCD camera and X-ray detector varied slightly among different acquisitions, leading to slight fluctuations (within several pixels) in the co-registration. Therefore, a registration algorithm that included the ability to adjust for variations in the conveyor speed and the time delay after an acquisition request during experiments was developed based on the simple image co-registration.

For a given rice kernel in the X-ray image, the registration algorithm found its matching spikelet hull in the LCCD image by using the following procedure:

Step 1: Sobel algorithm was performed to extract the boundary pixels of a given rice kernel, which were stored in a vector B. Length of the boundary vector B was calculated and denoted by T.
Step 2: An enumerator vector E was initialized to 0.
Step 3: An index variable t was initialized to 0.
Step 4: The corresponding point in the LCCD image (denoted by CB_t) of a given boundary pixel B_t (t = 1, 2, ..., T) was determined
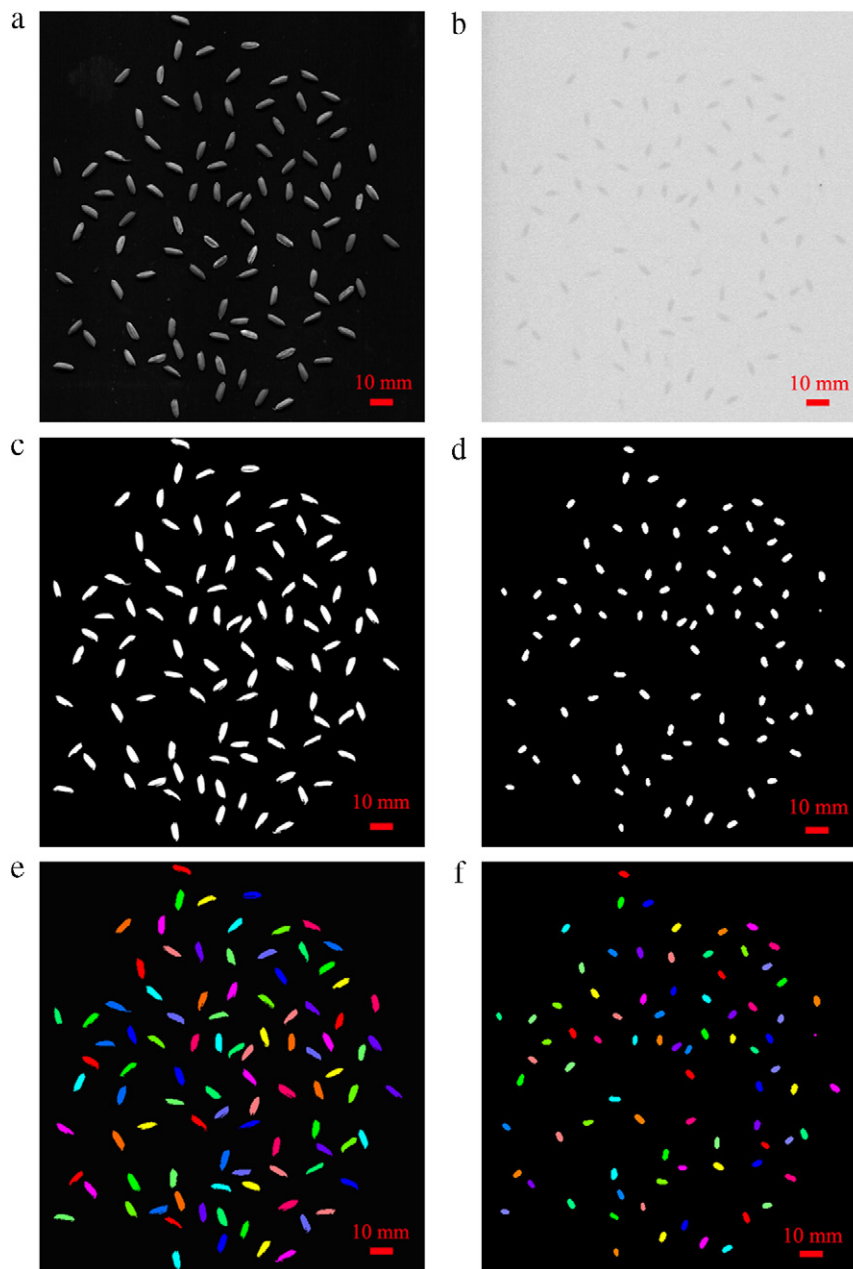
Fig. 4. Image processing procedural framework: (a) LCCD original image; (b) X-ray original image; (c) LCCD binary image; (d) X-ray binary image; (e) pseudo color image of LCCD labeled image; (f) pseudo color image of X-ray labeled image.

by the relative coordinates through simple co-registration. If CB_t had a non-zero pixel value j, the enumerator E_j was incremented ($j = 1, 2, \ldots, M$, where M was the number of objects in the LCCD image, i.e., total spikelet number).

Step 5: If t was equal to T, the procedure jumped to Step 6. Otherwise, the index t was incremented and the algorithm looped to Step 4.

Step 6: Let $j*$ be the labeling value of the corresponding spikelet hull of the given rice kernel such that

$$j* = \arg\max\{E_j | j = 1, 2, \ldots, M\} \qquad (1)$$

Fig. 5 illustrates the procedure of finding the matching spikelet hull of a rice kernel labeled by i. As shown in the image, E_k is larger than E_h, thus the spikelet hull labeled by k is deemed as the corresponding spikelet hull of rice kernel i.

Theoretically, all the pixels of a rice kernel can be used to determine its matching spikelet hull. However, for efficiency reasons, only boundary points were used in our method.

2.4.5. Unfilled and filled spikelets discrimination and counting

After the matching rice kernel-spikelet hull pairs were found, the filling rate (*FR*) of each spikelet was calculated by using the following equation:

$$FR = \frac{Area_{rice\ kernel}}{Area_{spikelet\ hull}} \qquad (2)$$

where $Area_{rice\ kernel}$ was the projected area of the rice kernel and $Area_{spikelet\ hull}$ was the projected area of its corresponding spikelet hull.

Specifically, an empty spikelet merely has a spikelet hull with no rice kernel inside and may appear in the LCCD image, whereas no matching rice kernel can be found in the X-ray image. In this
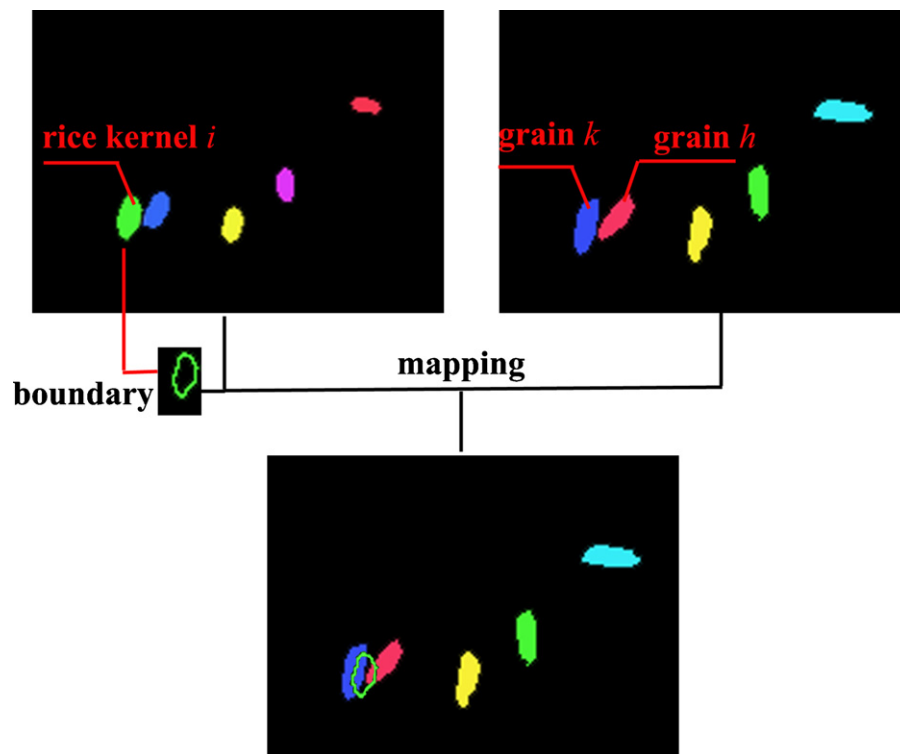
Fig. 5. Matching schematic diagram. Boundary points of a rice kernel are extracted and mapped to the LCCD image to find its corresponding spikelet.

case, the area of its matching rice kernel was assigned 0, which was in agreement with its practical property.

In a subsequent step, the filling rate of each spikelet was compared with a pre-defined threshold. If the filling rate of a spikelet was larger than the threshold, the spikelet was identified as a filled spikelet, otherwise it was assigned as unfilled. In the experiments, the threshold was set as 0.35, according to the preliminary experiments for an optimized performance.

In the end, the algorithm counted the filled spikelet number and the unfilled spikelet number.

2.5. Communication interface

The communication interface is indicated in Fig. 6. The labeled LCCD image and X-ray image, along with the number of filled spikelets, the number of unfilled spikelets, and the number of total spikelets, were displayed on the interface. The top-left button indicated whether the CCD camera and X-ray detector were acquiring images. The STOP button on the bottom-left corner was used for stopping the machine.

3. Results and discussion

3.1. Measurement accuracy

29 panicle samples were tested for accuracy of evaluation, from which absolute errors, defined as numbers measured using the present method minus the manually measured numbers, and relative errors, defined as absolute errors divided by manually measured numbers, were calculated.

Table 2 illustrates the total spikelet number, which was measured manually by expert workers and automatically by the present method. Absolute errors for the number of total spikelets were within ±1. The measured results for filled spikelet number are listed in Table 3. Compared with the measurement of the total spikelet number, absolute errors of filled spikelet number were a

little larger, between −2 and 1. The maximum absolute relative error was 1.56% for total spikelet number measurement, and 2.74% for filled spikelet number.

The root mean squared error (RMSE, defined by Eq. (3)) was 0.77 for filled spikelet number and 0.42 for total spikelet number. The

Table 2
Spikelets per panicle of 29 panicle samples measured manually versus by the present method.

| No.	Number measured automatically	Number measured manually	Absolute error	Relative error (%)
1	86	87	−1	−1.15
2	96	96	0	0.00
3	92	92	0	0.00
4	87	88	−1	−1.14
5	78	78	0	0.00
6	87	87	0	0.00
7	84	84	0	0.00
8	83	83	0	0.00
9	80	80	0	0.00
10	89	90	−1	−1.11
11	82	82	0	0.00
12	84	84	0	0.00
13	89	89	0	0.00
14	74	74	0	0.00
15	63	63	0	0.00
16	68	68	0	0.00
17	66	66	0	0.00
18	72	72	0	0.00
19	72	72	0	0.00
20	67	67	0	0.00
21	63	64	−1	−1.56
22	77	78	−1	−1.28
23	63	63	0	0.00
24	57	57	0	0.00
25	70	70	0	0.00
26	70	70	0	0.00
27	62	62	0	0.00
28	62	62	0	0.00
29	60	60	0	0.00
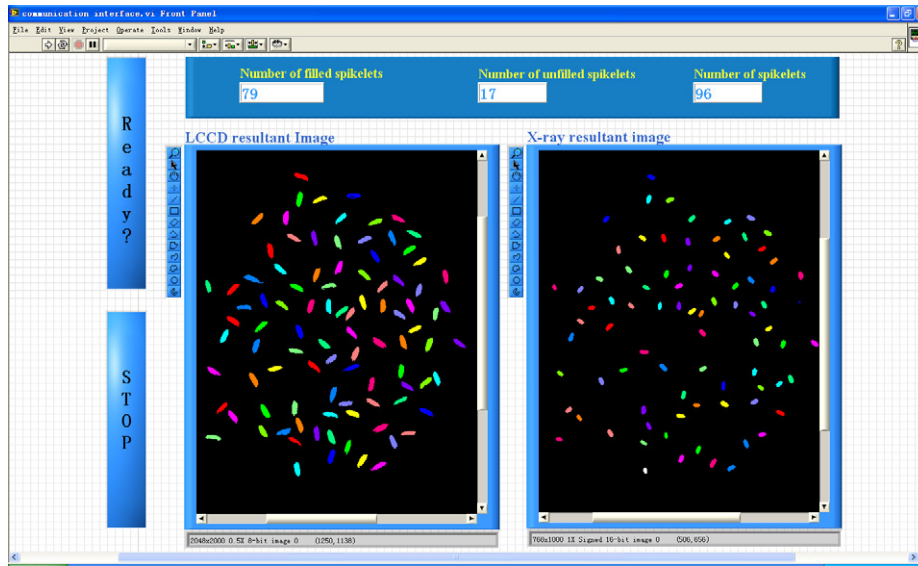
Fig. 6. Communication interface of the implemented prototype.

mean absolute percentage errors (MAPE, defined by Eq. (4)) were 0.80% and 0.22% for each, respectively.

$$\text{RMSE} = \sqrt{\frac{1}{n}\sum_{i=1}^{n}(X_{i.manual} - x_{i.image})^2} \tag{3}$$

$$\text{MAPE} = \frac{1}{n}\sum_{i=1}^{n}\frac{|X_{i.manual} - x_{i.image}|^2}{X_{i.manual}}100 \tag{4}$$

where $x_{i.manual}$ was the i_{th} manually measured value, $x_{i.image}$ was the i_{th} value measured using the present bi-modal imaging method, and n was the number of samples.

Table 3
Filled spikelets per panicle of 29 panicle samples measured manually versus by the present method.

No.	Number measured automatically	Number measured manually	Absolute error	Relative error (%)
1	71	73	−2	−2.74
2	79	80	−1	−1.25
3	83	82	1	1.22
4	75	76	−1	−1.32
5	71	70	1	1.43
6	79	78	1	1.28
7	73	73	0	0.00
8	76	75	1	1.33
9	74	74	0	0.00
10	71	71	0	0.00
11	76	76	0	0.00
12	73	73	0	0.00
13	78	78	0	0.00
14	65	65	0	0.00
15	58	58	0	0.00
16	60	60	0	0.00
17	60	61	−1	−1.64
18	58	58	0	0.00
19	58	59	−1	−1.69
20	62	62	0	0.00
21	54	55	−1	−1.82
22	63	63	0	0.00
23	57	56	1	1.79
24	50	49	1	2.04
25	62	62	0	0.00
26	61	61	0	0.00
27	56	56	0	0.00
28	55	54	1	1.85
29	53	52	1	1.92

Two main reasons may have led to the larger error in the measurement of filled spikelet number in comparison to the total spikelet number. First, incorrect discrimination may have occurred when the degree of filling for a filled spikelet was very close to that of an unfilled spikelet. Second, due to the low X-ray attenuation of rice spikelets, the contrast and SNR of X-ray image were relatively low in fast line-scan imaging, making it difficult to extract the rice kernel area precisely. More accurate measurements would be achieved if a higher performance X-ray system is used. Unfortunately, a higher performance X-ray system leads to higher cost, which is not suitable for wide-spread applications. With respect to the implemented prototype, counting accuracy was slightly larger due to the extra loss of spikelets caused by the conveying system.

3.2. Measurement efficiency

In order to optimize the measuring speed, images were processed in the computer simultaneously while the CCD camera and X-ray detector were acquiring new images. As image processing consumed less time than did image acquisition, the measurement efficiency of the present method was dictated by the speed of image acquisition.

We assume that the average length and width of a rice spikelet were 9 mm and 3 mm, respectively. In our experiments, the average space that a spikelet inhabited was approximately 300 mm^2 (11 times its size). Therefore, the number of spikelets/mm^2 (N_s) was 1/300 mm^2. The conveyor belt width was $W = 250$ mm and its velocity was $V = 40$ mm/s. Therefore, the number of spikelets passing through the CCD camera and X-ray detector per second was:

$$N_s V W = (\text{spikelets}/300\,\text{mm}^2)(40\,\text{mm/s})(250\,\text{mm})$$
$$= 33.3\,\text{spikelets/s} \tag{5}$$

This rate of detection corresponded to 2000 spikelets/min, which was the rate seen in our experiment. In practical measurements, the efficiency depends on the density of the spikelet kernels (N_s). If the N_s were increased to 1/108 mm^2 (space per grain = 4 times the area of grain), the rate of detection would be 5556 spikelets/min, which is a reasonable estimate of an optimized rate of detection. To further enhance efficiency, the conveyor belt could be broadened or the conveyor speed increased. However, a wider conveyor belt demands a larger field of view. A higher

conveyor speed decreases integration time, and therefore leads to lower SNR and contrast for X-ray image. When attempting to increase the rate of detection, care should be taken to not reduce the overall accuracy of filled and unfilled spikelets discrimination.

The results illustrate that the combination of visible light imaging and X-ray imaging can count filled spikelet number and total spikelet number simultaneously and automatically with acceptable accuracy. The length, width and other morphological features of rice spikelets were also acquired at the same time, opening up the possibility of including more traits in the prototype. A major limitation of this method is that the measurement efficiency and accuracy are influenced by the performance of the X-ray detector. Higher accuracy and efficiency would be achieved given a higher performance X-ray system. In the current prototype, a manual pressing of a control button triggered image acquisition. Future designs could utilize a photoelectric sensor as an external trigger to automate image acquisition.

4. Conclusions

This paper demonstrates a new method for simultaneously and efficiently acquiring the number of filled spikelets, the number of unfilled spikelets, and the number of total spikelets. Bi-modal imaging using visible light imaging and soft X-ray imaging was employed in a method for fast discrimination of filled spikelets and unfilled spikelets. This method simultaneously measures filled spikelet number and total spikelet number without manual separation of spikelets, which significantly improves the efficiency of trait evaluation in rice breeding and genetic research. A fully automated spikelet counting machine, which is capable of simultaneously measuring the filled spikelet number, unfilled spikelet number, total spikelet number as well as spikelet dimension (length and width), will be developed in the future. Other cereal grains, such as wheat, will be also used as samples. The newly developed device will serve as a tool for phenomics research, which aims to usher "precision agriculture and predictive breeding" (Finkel, 2009).

Acknowledgements

References

Bohra, J.S., Doerffling, K., 1993. Potassium nutrition of rice (*Oryza sativa* L.) varieties under NaCl salinity. Plant and Soil 152, 299–303.

Bueno, C.S., Lafarge, T., 2009. Higher crop performance of rice hybrids than of elite inbreds in the tropics. Field Crops Research 112, 229–237.

Crowe, T., Luo, X., Jayas, D., Bulley, N., 1997. Color line-scan imaging of cereal spikelet kernels. Applied Engineering in Agriculture 13 (5), 689–694.

Finkel, E., 2009. With 'Phenomics,' plant scientists hope to shift breeding into overdrive. Science 325, 380–381.

Fornal, J., Jeliński, T., Sadowska, J., Grundas, S., Nawrot, J., Niewiada, A., Warchalewski, J.R., Błaszczak, W., 2007. Detection of granary weevil *Sitophilus granarius* (L.) eggs and internal stages in wheat spikelet using soft X-ray and image analysis. Journal of Stored Products Research 43 (2), 142–148.

Haff, R.P., Slaughter, D.C., 2004. Real-time X-ray inspection of wheat for infestation by the granary weevil, *Sitophilus Granarius* (L.). Transaction of ASAE 47 (2), 531–537.

Karunakaran, C., Jayas, D.S., White, N.D.G., 2004. Detection of internal wheat seed infestation by *Rhyzopertha dominica* using X-ray imaging. Journal of Stored Products Research 40, 507–516.

Lian, X., Xing, Y., Yan, H., Xu, C., Li, X., Zhang, Q., 2005. QTLs for low nitrogen tolerance at seedling stage identified using a recombinant inbred line population derived from an elite rice hybrid. Theoretical and Applied Genetics 112, 85–96.

Luo, X., Jayas, D., Symons, S., 1999. Identification of damaged kernels in wheat using a color machine vision system. Journal of Cereal Science 30, 49–59.

Manickavasagan, A., Sathya, G., Jayas, D.S., White, N.D.G., 2008. Wheat class identification using monochrome images. Journal of Cereal Science 47, 518–527.

Neethirajan, S., Jayas, D., Karunakaran, C., 2007a. Dual energy X-ray image analysis for classifying vitreousness in durum wheat. Postharvest Biology and Technology 45, 381–384.

Neethirajan, S., Jayas, D., White, N., 2007b. Detection of sprouted wheat kernels using soft X-ray image analysis. Journal of Food Engineering 81, 509–513.

Paglieroni, D., 1992. Distance transforms: properties and machine vision applications. Computer Vision, Graphics, and Image Processing: Graphical Models and Image Processing 54 (1), 57–58.

Prasertsak, A., Fukai, S., 1997. Nitrogen availability and water stress interaction on rice growth and yield. Field Crops Research 52, 249–260.

Thomson, M.J., Tai, T.H., McClung, A.M., Lai, X.-H., Hinga, M.E., Lobos, K.B., Xu, Y., Martinez, C.P., McCouch, S.R., 2003. Mapping quantitative trait loci for yield, yield components and morphological traits in an advanced backcross population between *Oryza rufipogon* and the *Oryza sativa* cultivar Jefferson. Theoretical and Applied Genetics 107, 479–493.

Tian, F., Li, D., Fu, Q., Zhu, Z., Fu, Y., Wang, X., Sun, C., 2006. Construction of introgression lines carrying wild rice (*Oryza rufipogon* Griff.) segments in cultivated rice (*Oryza sativa* L.) background and characterization of introgressed segments associated with yield-related traits. Theoretical and Applied Genetics 112, 570–580.

Tirol-Padre, A., Ladha, J., Singh, U., Laureles, E., Punzalan, G., Akita, S., 1996. Grain yield performance of rice genotypes at suboptimal levels of soil N as affected by N uptake and utilization efficiency. Field Crops Research 46, 127–143.

Venora, G., Grillo, O., Saccone, R., 2009. Quality assessment of durum wheat storage centres in Sicily: evaluation of vitreous, starchy and shrunken kernels using an image analysis system. Journal of Cereal Science 49, 429–440.

Vincent, L., Soille, P., 1991. Watersheds in digital spaces: an efficient algorithm based on immersion simulations. IEEE Transactions on Pattern Analysis and Machine Intelligence 13 (6), 583–598.

Vincent, L., 1992. Morphological grayscale reconstruction: definition, efficient algorithm and applications in image analysis. Proceedings of Computer Vision and Pattern, 633–635.

Vincent, L., 1993. Morphological grayscale reconstruction in image analysis: applications and efficient algorithms. IEEE Transactions on Image Processing 2 (2), 176–201.

Wan, Y., Lin, C., Chiou, J., 2002. Rice quality classification using an automatic spikelet quality inspection system. Transactions of the ASAE 45 (2), 379–387.

Wang, E., Wang, J., Zhu, X., Hao, W., Wang, L., Li, Q., Zhang, L., He, W., Lu, B., Lin, H., Ma, H., Zhang, G., He, Z., 2008. Control of rice spikelet-filling and yield by a gene with a potential signature of domestication. Nature Genetics 40 (11), 1370–1374.

Xiao, J., Li, J., Grandillo, S., Ahn, S.N., Yuan, L., Tanksley, S.D., McCouch, S.R., 1998. Identification of trait-improving quantitative trait loci alleles from a wild rice relative, *Oryza rufipogon*. Genetics 150, 899–909.

Xing, Y., Zhang, Q., 2010. Genetic and molecular bases of rice yield. Annual Review of Plant Biology 61, 11.1–11.22.

Yang, J., Peng, S., Visperas, R., Sanico, A., Zhu, Q., Gu, S., 2000. Spikelet filling pattern and cytokinin content in the spikelets and roots of rice plants. Plant Growth Regulation 30, 261–270.

Yang, J., Zhang, J., Wang, Z., Zhu, Q., 2001. Activities of starch hydrolytic enzymes and sucrose-phosphate synthase in the stems of rice subjected to water stress during grain filling. Journal of Experimental Botany 52 (64), 2169–2179.

Ying, J., Peng, S., He, Q., Yang, H., Yang, C., Visperas, R.M., Cassman, K.G., 1998. Comparison of high-yield rice in tropical and subtropical environments. I. Determinants of grain and dry matter yields. Field Crops Research 57, 71–84.

Yoshida, S., 1981. Fundamentals of Rice Crop Science. International Rice Research Institute, Los Baños, Philippines, p. 61.

Zayas, I., Pomeranz, Y., Lai, F., 1989. Discrimination of wheat and nonwheat components in grain samples by image analysis. Cereal Chemistry 66 (3), 233–237.

Zhang, Q., 2007. Strategies for developing green super rice. PNAS 104 (42), 16402–16409, http://www.seedburo.com/prod_lit/categ07/CountAPak07lit.pdf.